Article

Precipitation observing network gaps limit climate change impact assessment

https://doi.org/10.1038/s41586-026-10300-5

Received: 18 July 2025

Accepted: 19 February 2026

Published online: 25 March 2026

Open access

Check for updates

Jiajia Su[1], Chiyuan Miao[1]✉, Francis Zwiers[2,3], Hylke Beck[4], Phil Jones[5], Qiaohong Sun[2], Louise J. Slater[6], Wouter R. Berghuijs[7], Yoshihide Wada[8], Daniel Rosenfeld[9], Jiaojiao Gou[1], Yi Wu[1], Paolo Tarolli[10], Pasquale Borrelli[11,12], Panos Panagos[13], Lisa V. Alexander[14], Qi Zhang[1,15], Jinlong Hu[1], Seung-Ki Min[16], Luis Samaniego[17,18], Qingyun Duan[19], Georgia Destouni[20,21,22], Jose A. Marengo[23,24,25], Reza Modarres[26] & Soroosh Sorooshian[27]

Reliable future climate projections and water deficiency assessments require precipitation observations that are both spatially comprehensive and temporally complete, yet many global regions still suffer from observation sparsity[1,2]. Here we evaluate the distribution of 221,483 internationally exchanged precipitation gauges worldwide, with records across 1900–2022, and further explore where new gauges are most needed under different scenarios. We find that at present only 13.4% of the global land surface meets the World Meteorological Organization requirements for annual precipitation monitoring, indicating widespread scarcity that has serious socioeconomic implications. Europe has the highest continental gauge density (2.4 gauges per 1,000 km^2), with Germany leading among countries over 50,000 km^2 (22.4 gauges per 1,000 km^2). Globally, 25% of land surface already requires urgent expansion of gauge networks because of climate variability, including northern South America, northern North America, Central Africa and southern Asia. Considering projected precipitation changes and socioeconomic conditions under a high-emission scenario further identifies high-need regions in India, Greenland, Bolivia and China because of climate sensitivity and socioeconomic vulnerabilities, increasing this share to 32.1% of global land. Our findings highlight important gaps in global precipitation monitoring that require strategic investments in new gauges and underscore the need for open data access.

Precipitation is an important component of the global water cycle, affecting both ecological systems and human society. It is the primary source of freshwater[3], accounting for approximately 84–90% of global water consumption[4]. Precipitation deficits have marked impacts on agricultural and urban areas, with nearly 80% of the population of the world (as of 2000) facing water security issues[5]. Furthermore, terrestrial habitats and biodiversity may be compromised by changes in precipitation variability under global warming[5–9]. Future projections indicate a substantial increase in precipitation variability over 2071–2100, affecting approximately 66% of the global land surface[10]. This heightened variability results from the intensification of precipitation extremes[11], which amplifies climatic and hydrological extremes[12,13], including floods[14,15], droughts[16] and the combined effects of wet and dry events with temperature rise[17,18]. Extreme events, such as devastating flooding in Valencia (29 October 2024) and Germany (14 and 15 July 2021) that caused many casualties, massive disruption and economic losses, reinforce the need for monitoring climate change effects on the terrestrial water systems.

[1]State Key Laboratory of Earth Surface Processes and Disaster Risk Reduction, Faculty of Geographical Science, Beijing Normal University, Beijing, China. [2]State Key Laboratory of Climate System Prediction and Risk Management/Key Laboratory of Meteorological Disaster, Ministry of Education/Collaborative Innovation Center on Forecast and Evaluation of Meteorological Disasters, Nanjing University of Information Science and Technology, Nanjing, China. [3]Pacific Climate Impacts Consortium, University of Victoria, Victoria, British Columbia, Canada. [4]Physical Science and Engineering Division, King Abdullah University of Science and Technology, Thuwal, Saudi Arabia. [5]Climatic Research Unit, School of Environmental Sciences, University of East Anglia, Norwich, Norfolk, UK. [6]School of Geography and the Environment, University of Oxford, Oxford, UK. [7]Department of Earth Sciences, Vrije Universiteit Amsterdam, Amsterdam, The Netherlands. [8]Biological and Environmental Science and Engineering Division, King Abdullah University of Science and Technology, Makkah, Saudi Arabia. [9]Institute of Earth Sciences, The Hebrew University of Jerusalem, Jerusalem, Israel. [10]Department of Land, Environment, Agriculture and Forestry, Università degli Studi di Padova, Legnaro, Italy. [11]Environmental Modeling and Global Change Lab, Department of Science, Roma Tre University, Rome, Italy. [12]Department of Environmental Sciences, Environmental Geosciences, University of Basel, Basel, Switzerland. [13]European Commission, Joint Research Centre (JRC), Ispra, Italy. [14]Climate Change Research Centre and ARC Centre of Excellence for Weather of the 21st Century, UNSW Sydney, Sydney, Australia. [15]Qinghai Province Key Laboratory of Physical Geography and Environmental Process, College of Geographical Science, Qinghai Normal University, Xining, China. [16]Division of Environmental Science and Engineering, Pohang University of Science and Technology, Pohang, South Korea. [17]Department of Computational Hydrosystems, Helmholtz Centre for Environmental Research—UFZ, Leipzig, Germany. [18]Institute of Environmental Science and Geography, University of Potsdam, Potsdam, Germany. [19]State Key Laboratory of Water Disaster Prevention, College of Hydrology and Water Resources, Hohai University, Nanjing, China. [20]Department of Physical Geography, Stockholm University, Stockholm, Sweden. [21]Department of Sustainable Development, Environmental Science and Engineering, KTH Royal Institute of Technology, Stockholm, Sweden. [22]Stellenbosch Institute for Advanced Study, Stellenbosch, South Africa. [23]Centro Nacional de Monitoramento e Alertas de Desastres Naturais, CEMADEN, São José dos Campos, Brazil. [24]UNESP/CEMADEN, São José dos Campos, Brazil. [25]Graduate School of International Studies, Korea University, Seoul, South Korea. [26]Department of Natural Resources, Isfahan University of Technology, Isfahan, Iran. [27]Center for Hydrometeorology and Remote Sensing, Department of Civil and Environmental Engineering, University of California, Irvine, Irvine, CA, USA. ✉e-mail: miaocy@bnu.edu.cn

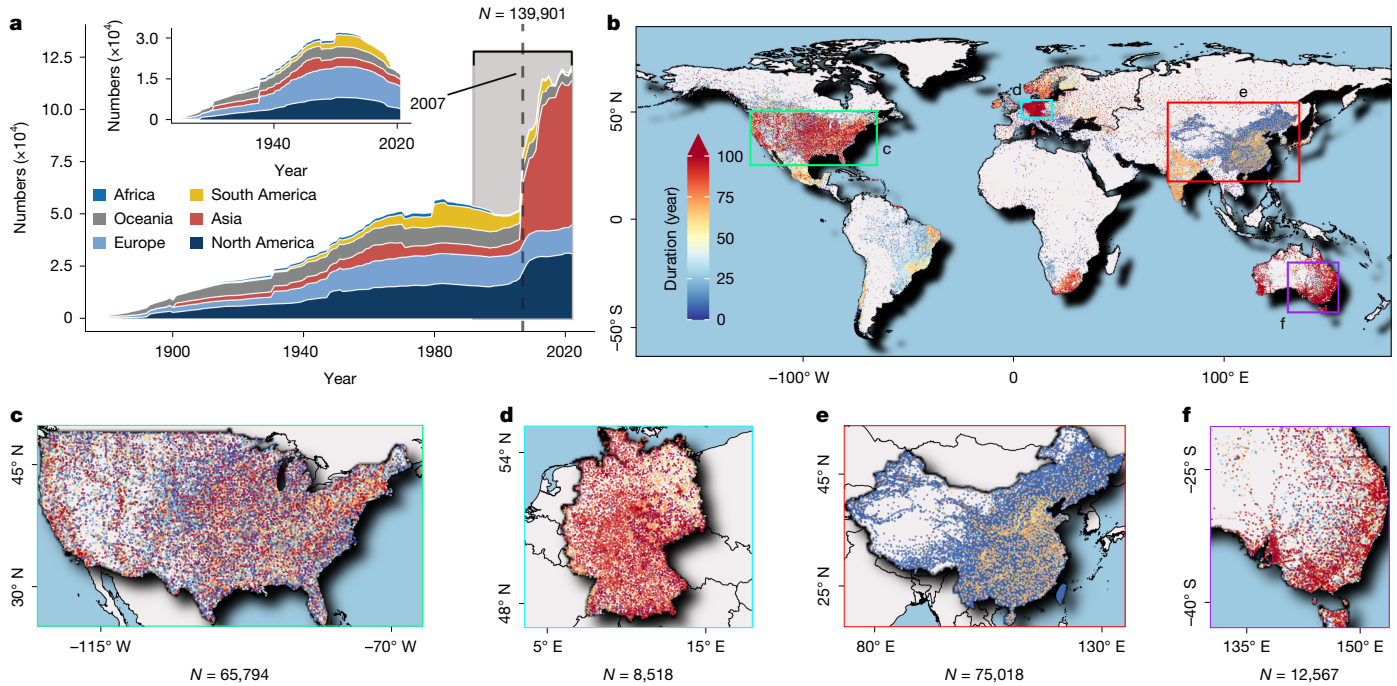

Fig. 1 | Collected daily precipitation gauge records from 1900 to 2022 (221,483 gauges). a, Yearly count of stations by continent. The stacked area plot inset presents the yearly count of LR stations (38,203 gauges) meeting specific criteria (Methods). **b**–**f**, Map of stations record lengths (**b**), with focusing on four regions: the United States (**c**), Germany (**d**), China (**e**) and Southeast Australia (**f**), with notable precipitation gauge densities. The bottom numbers indicate the station numbers within the four regions. The map image is the intellectual property of Esri and is used herein under license. Copyright © 2026 Esri and its licensors. All rights reserved.

Reliable estimates of change in historical and future terrestrial precipitation rely on the availability of precipitation observations. At present, methods for capturing the observed spatiotemporal distribution of precipitation include indirect approaches (primarily radar and satellite technologies[19,20]) and direct methods (in situ observational instruments[21]). Although radar and satellite technologies provide valuable, spatially continuous and high-frequency temporal data, they also have limitations, including systematic biases, sensitivity to synoptic regimes[20,22], estimation errors[23,24] and economic constraints[25]. Reanalysis products provide longer records than satellites, but their precipitation estimates remain uncertain globally[26], especially in the tropics[27]. By contrast, precipitation gauges offer ground-level measurements with greater accuracy[28,29], making them essential for estimating regional precipitation and water resources[30–32], but their availability is limited[1,2].

As the primary instrument for precipitation measurement, rain gauges were widely installed through the efforts of organizations such as the World Meteorological Organization (WMO) and national meteorology institutions worldwide, particularly before the 1980s. However, the reliability and availability of precipitation data have declined since then due to factors such as the lack of data sharing by hydrometric authorities[33], the dissolution of the Soviet Union[34] and economic conflicts during the twentieth century[35], resulting in much more limited coverage than during the 1980s. A striking example of this limited coverage is the Global Precipitation Climatology Centre (GPCC)—one of the most widely used precipitation datasets—for which, in 2015, only 1.6% of the surface of Earth was within 10 km of an operational precipitation gauge[1,2]. Reliable and accessible precipitation datasets are crucial for numerous scientific endeavours, such as the study of extreme climate events[36–38], runoff patterns[39], evapotranspiration[40], ecosystem respiration[41], soil erosion[42], sediment fluxes[43], climate-agriculture interactions[44], spatial planning[45], climate impacts on food[46] and energy production[47], fire risk[48] and carbon sequestration dynamics[49,50]. Given the importance of these factors, it is essential to conduct a comprehensive evaluation of precipitation gauge networks to better inform network management and planning so that the gauge networks contribute effectively to the monitoring of climate change across the globe.

This study uses publicly available global and national precipitation gauge datasets, comprising 221,483 gauges from 1900 to 2022. We investigate the global distribution of gauges across physiographic regions, comparing them with the station density standards set by the WMO. Moreover, we consider current gauge density, characteristics of historical precipitation changes, future precipitation change scenarios and future socioeconomic conditions to identify regions in which new gauges are needed. If deployed, these additional gauges would play a vital part in improving climate services in many areas, effectively monitoring precipitation changes, advancing our understanding of past and future climate changes, and supporting further research on the water cycle and climate change projections.

Spatiotemporal variability of global gauge records

Between 1900 and 2022, observations from 221,483 accessible precipitation gauges were recorded (Supplementary Table 1), of which 63.2% (139,901) remained active within the past 30 years, indicating insufficient recent observations coverage. From 1900 to the 1980s, both the number of stations and long-term record (LR) stations—defined as stations with records spanning more than 30 years and less than 10% missing data—grew globally (Fig. 1a), but their trends varied regionally thereafter.

A slight increase in the total number of stations occurred in 1983 following the global rollout of automatic precipitation gauges in 1982 that occurred after the WMO introduced standard non-recording precipitation gauge measurements in 1981 (refs. 51,52). Asia saw a notable surge in station numbers that was largely driven by the sustained efforts of China to deploy automatic rain gauges beginning in that period[53]. Consequently, Asia had nearly 70,000 precipitation gauges by 2022, comprising roughly 57.2% of the global total and representing

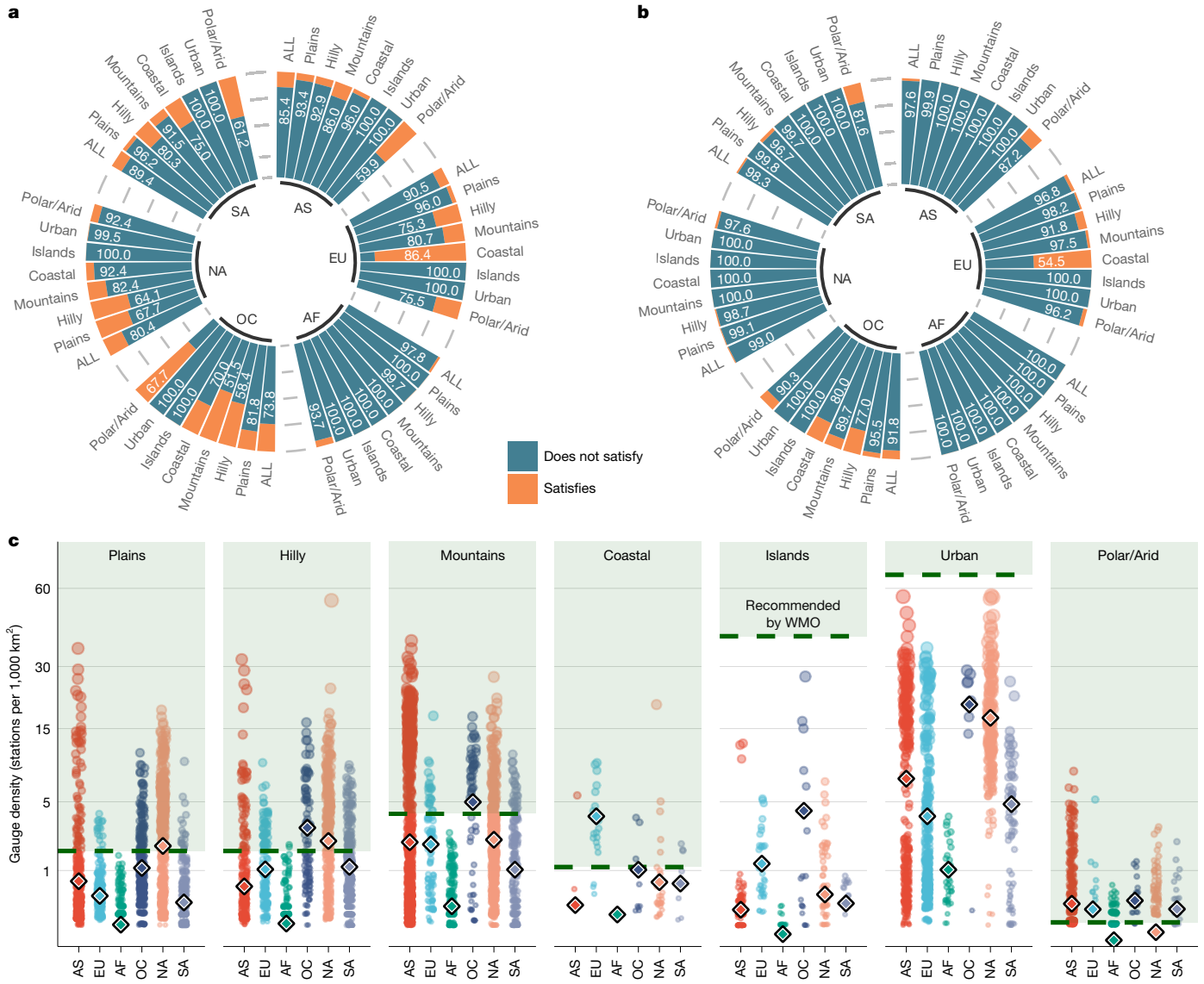

Fig. 2 | Global precipitation gauge density during 1900–2022 compared with WMO standards. a,**b**, The circular bar plot indicates the proportion of each physiographic region, in which the density of stations (**a**) or LR stations (**b**) meets (orange) or does not meet (blue) WMO requirements. The higher proportion is labelled within each bar. Continental abbreviations are as follows: AS, Asia; EU, Europe; AF, Africa; OC, Oceania; NA, North America; and SA, South America. **c**, Station density. Bubbles indicate grid-cell gauge densities, whereas diamonds represent the mean density for each continent and physiographic region. Horizontal dashed green lines represent the minimum density recommendations of WMO for each physiographic region. Gauge density is based on a 1° × 1° grid for the period 1900–2022.

the largest share of any region (Supplementary Table 2). Although stations in Asia have relatively short record lengths (Fig. 1, Supplementary Fig. 1), they hold marked potential for future climate monitoring if they continue to operate. North America also experienced a sharp rise in gauge numbers in the 2000s, reaching over 30,000 by 2022 (25.6% of global total, ranked second). By contrast, the consistent decline in the total number of stations across most other continents does not bode well for long-term data availability, pointing to a heightened risk of future observational scarcity.

Although LR stations make up only a much smaller fraction of all stations, their proportion provides a clearer indicator of current long-term data availability. Since the 1980s, the number of LR stations has generally declined, primarily due to limited data sharing[33], the dissolution of the Soviet Union[34] and the twentieth-century economic conflicts[35], all of which restricted data accessibility and usability. By 2022, only 16,491 (13.8%) of 119,731 operating stations were LR stations. Europe had the largest share (49.8%, 8,205 stations), whereas North America (23.6%, 3,892 stations) and Asia (15.9%, 2,623 stations) mainly accounted for the remaining LR stations (Supplementary Table 2). The global scarcity of LR stations that has developed since the 1980s, and similar trends in river gauge availability[35] limits the effectiveness of long-term climate change monitoring and should be a serious concern for policymakers and researchers.

The availability of global precipitation gauges exhibits considerable spatial heterogeneity (Fig. 1b and Supplementary Fig. 2). Germany and Austria lead the station density and LR station density ranking for countries with areas exceeding 50,000 km² (Extended Data Fig. 1). European countries have the highest densities of all stations (2.4 stations per 1,000 km²), followed by North America (1.1 stations per 1,000 km²). For LR stations, European again has the highest density (1.3 stations per 1,000 km²), exceeding second-place Oceania (0.2 stations per 1,000 km²) by nearly an order of magnitude (Supplementary Table 2). This severe shortage of long-term observations underscores the challenge to the track water cycle and predict future

weather events more accurately, especially in Africa (where the total and LR station densities are 0.09 and 0.02 stations per 1,000 km^2, respectively).

Comparison of gauge density with WMO requirements

The surface physical features of Earth strongly influence the spatial variability of precipitation. In 1992, the WMO defined minimum gauge density requirements for annual precipitation observations for different physiographic regions[54,55] (Supplementary Table 3 and Supplementary Fig. 3). Our results show that only 13.4% of global land meets the recommended station density between 1900 and 2022, dropping to just 1.9% for LR stations only (Fig. 2). This indicates current global gauge density is insufficient for annual and seasonal precipitation monitoring. For example, Oceania has the highest percentage of land area satisfying the recommended standards of WMO, although only 26.2% of the territory reaches the threshold. The situation is more concerning for LR stations (Fig. 2b), apart from Oceania, where more than 5% of land meets the density target, the recommended threshold is largely unmet on other continents. The insufficient of gauge density can be attributed to limited publicly data accessibility[2], high cost of network construction and maintenance, challenges in ensuring data quality and homogeneity[56], and lower prioritization in regions perceiving limited climate risks[1]. Given the essential role of LR stations in monitoring climate-induced changes in water availability, this scarcity raises serious concerns for long-term hydrological observation.

The Polar/Arid region stands out as the sole physiographic category, in which, across most continents, the mean station density closely meets WMO standards (0.1 stations per 1,000 km^2), probably because of the relatively low spatial variability of precipitation in these areas (Fig. 2c). Notably, station density is highly uneven across Polar/Arid regions themselves, a high concentration of gauges in some specific areas. In Polar/Arid regions of Europe, for instance, the average density exceeds the WMO requirements (Fig. 2c), and only 24.5% of sub-regions actually surpasses the recommendation (Fig. 2a). Moreover, the physiographic Arctic-polar region is much smaller than the hydrologically relevant total Pan-Arctic Drainage Basin (PADB) that feeds the freshwater from land into the Arctic Ocean. The PADB includes many different physiographic, ecological, climatic and other regional characteristics within its total area of approximately 22.4 million km^2, and it has been shown that the existing hydrological monitoring data are too limited to be representative of the PADB as a whole[57].

The Small Islands (excluding nearby ocean areas) and Urban regions require particular attention as the only regions with mean station densities consistently below the WMO threshold. However, Small Islands are susceptible to sea-level rise and coastal extremes, play a key part in climate mitigation[58] and face isolation challenges comparable to urban sprawls[59,60]. At the same time, Urban regions, with their dense populations, impervious surfaces and rapid drainage, need fine-scale monitoring of extremes such as flash floods, especially under rapid urbanization[61]. As a result, both overall station and LR station densities are at present insufficient worldwide (Extended Data Fig. 2 and Supplementary Fig. 4). This highlights the challenge of obtaining comprehensive and representative precipitation information. To address this issue—especially the important question of where additional gauges are most needed—we explicitly integrated historical precipitation observations, future precipitation projections and future socioeconomic factors to ensure that the final priority rankings reflect regional needs, as shown in Extended Data Fig. 3.

Priority areas under historical period

Assessing current gauge density and precipitation spatial variability offers a benchmark for identifying priority areas for siting new gauges, expressed as PSNG values ranging from 1 (lowest priority) to 8 (highest priority) (Methods). High PSNG indicates a combination of high precipitation spatial variability and low gauge density, implying insufficient monitoring. Precipitation spatial variability is derived from daily precipitation records from LR stations using an entropy method that evaluates the information content of precipitation observations and its redundancy relative to neighbouring stations. PSNG is determined from gauge density and spatial variability using two weighting methods: the entropy weight method (dispersion-based information content) and principal component analysis (variance-structure considerations). During the historical period, there is good correspondence between areas with low PSNG and those that meet WMO observing station density standards and vice versa (Fig. 3a and Supplementary Fig. 4).

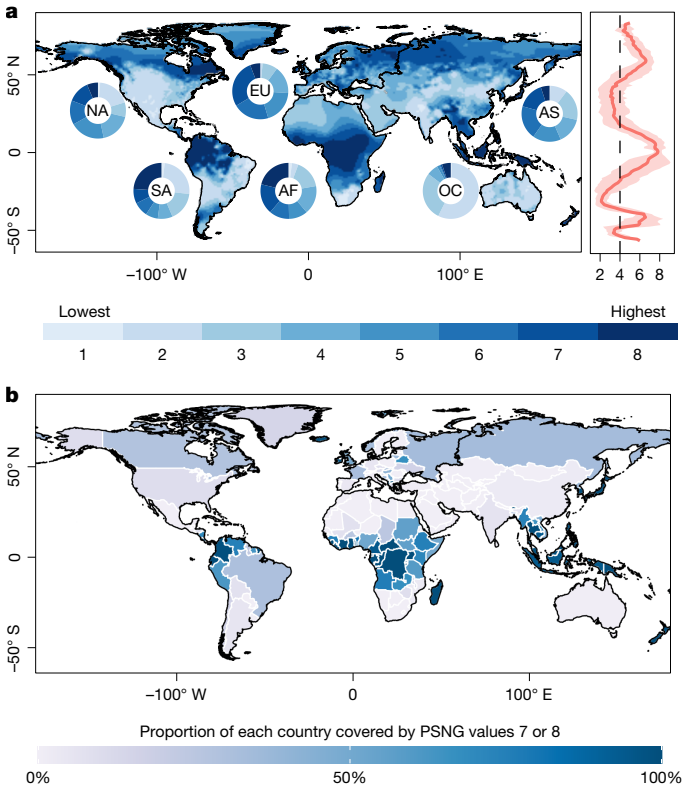

Fig. 3 | Global priority for siting new gauges (PSNG) under historical period (1900–2022). a, The inset pie charts show the relative proportion of each PSNG level across continents. The red line on the right represents the mean PSNG by latitude, with shading for the mean ± 1 standard deviation. Continental abbreviations are as follows: AS, Asia; EU, Europe; AF, Africa; OC, Oceania; NA, North America; and SA, South America. **b**, Proportion of each country covered by PSNG levels 7–8. The map image is the intellectual property of Esri and is used herein under license. Copyright © 2026 Esri and its licensors. All rights reserved.

Globally, approximately 25% of land areas are identified as high priority for siting new gauges (PSNG score of 7–8) based on historical precipitation information from 1900 to 2022 (Fig. 3a and Supplementary Fig. 5). This includes extensive parts of Africa (38.7% of the land area of the continent), South America (32.3%) and Europe (33.6%). High priority arises in these regions because of different reasons. High priority in low-latitude regions is often due to a combination of highly variable daily precipitation and low inter-station redundancy. For example, in Central Africa and northern South America, the key mechanisms producing high variability are often associated with their monsoon regimes, including a strong land–ocean thermal contrast[62], and the annual movement of active convective zones (for example, the South Atlantic and Intertropical Convergence Zones). Also, variability in these regions can be further modulated by slow changes in the Atlantic Meridional Overturning Circulation[63,64]. High priority in

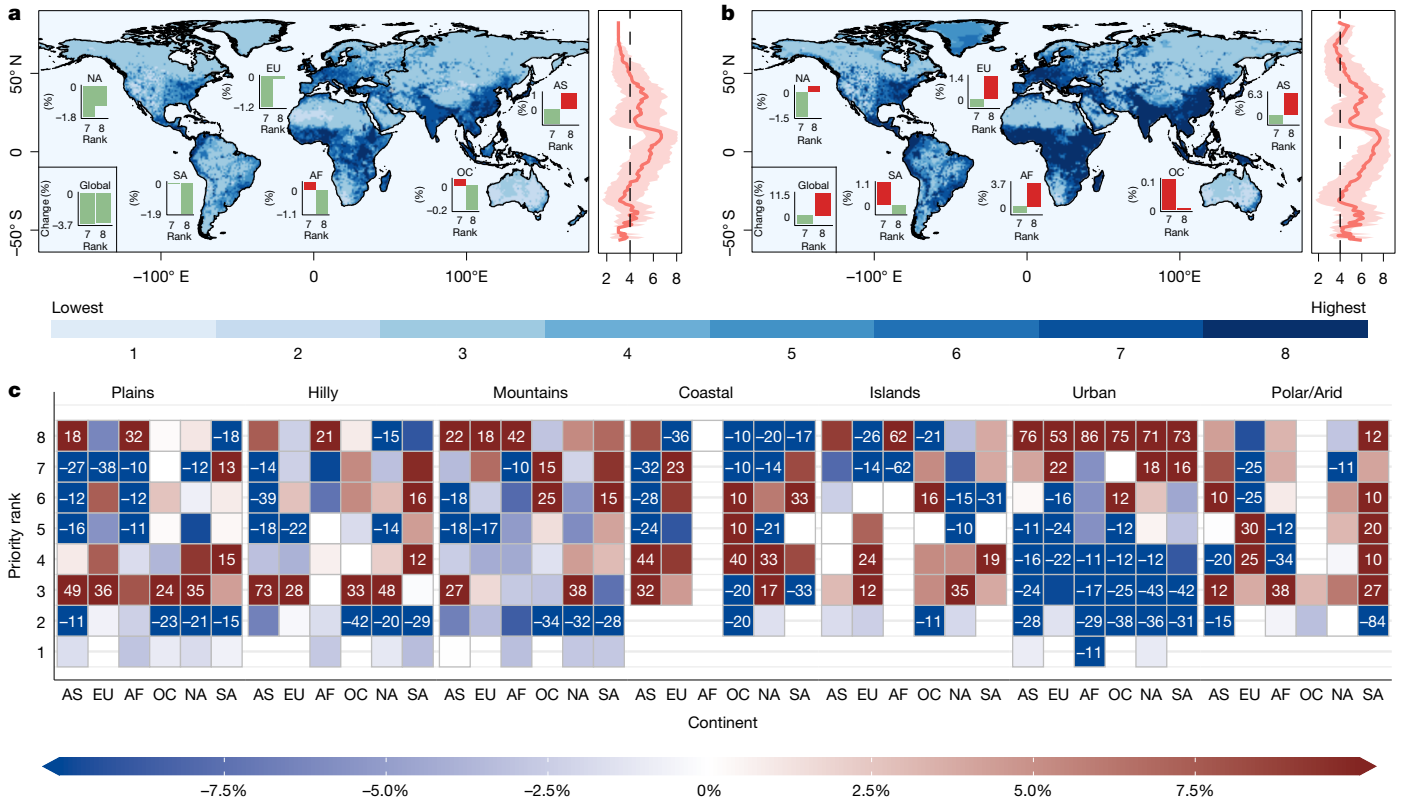

Fig. 4 | Global gauge-siting priority under future period. a,**b**, Spatial distribution of PSNG derived under future (2025–2100) SSP1-2.6 (**a**) and SSP5-8.5 (**b**) scenarios. Inset bar charts compare future and historical proportions of high PSNG levels (7–8) globally and by continent, with red and green representing increases and decreases, respectively. The red line shows mean PSNG by latitude, with shading indicating the mean ± 1 standard deviation. **c**, Projected changes relative to historical PSNG by physiographic region and continent, with values above 10% highlighted. Continental abbreviations are as follows: AS, Asia; EU, Europe; AF, Africa; OC, Oceania; NA, North America; and SA, South America. The map image is the intellectual property of Esri and is used herein under license. Copyright © 2026 Esri and its licensors. All rights reserved.

high-latitude regions, including Northern Europe, is driven primarily by Arctic amplification, rapid sea ice retreat, annul snow fraction changes[65,66] in warming climate, and compounded in Europe by the influence of the North Atlantic Oscillation[67]. Additional gauges in these northern areas would enhance the understanding of the global water cycle, as the sparse network of available stations complicates model bias evaluation[68] and inhibits the ability to understand how warming and precipitation changes are reshaping the hydrology of many cold regions[69,70]. By contrast, Asia (20.7%) exhibits substantial inter-station redundancy, leading to low priority despite high precipitation variability associated with the Asian monsoon[63].

National-level analysis identifies 106 countries with the most urgent need for new precipitation gauges (Fig. 3b). Among them, 63 countries are denoted as hotspot countries, in which more than 50% of the territory is high PSNG zones. For example, large countries (more than 500,000 km^2) include the Central African Republic (population 5.5 million in 2025), Democratic Republic of Congo (112.8 million), Madagascar (32.7 million), Colombia (53.4 million) and Indonesia (285.7 million). Note that increasing data accessibility to provide access to existing gauges may be a very cost-efficient way of reducing PSNG in some high-priority areas, including the nations of Europe[71] or Asia[72].

PSNG also exhibits notable regional variations across physiographic regions, shaping our understanding of climate change and water stress in specific regions (Supplementary Fig. 6), such as the Small Islands in Asia and Europe, and Costal Zones in Europe, Africa and Oceania, which show more than half of physiographic regions rank as high PSNG, probably because of enhanced land–ocean temperature contrasts[62]. The spatial patterns in PSNG distribution are insensitive to the spatial (0.5°, 2.5°, 5°) and temporal (1990–2022) resolution (Extended Data Fig. 4 and Supplementary Fig. 7). Moreover, random gauge reduction experiments in North America supporting PSNG utility in guiding the placement of new stations (Extended Data Fig. 5, Supplementary Text 9 and Supplementary Fig. 8).

Priority areas under future scenarios

Future precipitation projections suggest that PSNG will shift to higher values as climate warming increases the spatial variability of precipitation[7,73,74], reducing the mutual information shared among existing stations, a change quantified by analysing the uncertainty in CMIP6-based precipitation trend projections. We isolated the impact of precipitation by evaluating PSNG using future precipitation under low-emission and high-emission forcing scenarios (Shared Socioeconomic Pathway SSP1-2.6 and SSP5-8.5; Methods). The result indicates regional deviations with historical distributions (Supplementary Text 10 and Supplementary Figs. 9–14). Beyond precipitation, future socioeconomic conditions further affect PSNG by altering the relative prosperity of difference regions, and thus their ability to install and maintain stations, and by increasing the need for denser gauge networks in highly populated regions. By simultaneously considering future projections of both precipitation and socioeconomic conditions (2025–2100) under SSP1-2.6 and SSP5-8.5, we found that 32.1% of the land area of Earth falls into the high PSNG category under SSP5-8.5, compared with 17.7% under SSP1-2.6 (Fig. 4). The resulting spatial distribution differs from that based only on historical precipitation-related factors (Fig. 3), with additional high-priority areas identified in eastern–southern North America, western–southern Europe and southern Asia (Fig. 4).

Under the SSP5-8.5 scenario, precipitation dynamics and socioeconomic pressures converge to elevate the PSNG in both low- and mid-latitude regions (Extended Data Fig. 6 and Supplementary Fig. 15). Low-latitude areas in Africa and South America exhibit the most extensive coverage of high PSNG land area, with 54.9% and 39.3% of their respective continental areas classified as high priority, corresponding to increases of 16.3% and 7.0%, respectively, compared with the historical period (Supplementary Fig. 5). These areas are particularly sensitive to precipitation variability governed by monsoon systems and convective activity[62–64]. By contrast, across Europe, Asia and North America, socioeconomic factors dominantly amplify PSNG, with high-priority area expansions reaching 43.6%, 31.4%, and 14.4%, respectively. This pattern is generally evident in high-population or high-GDP nations. For instance, when socioeconomic dimensions are incorporated, France (population 66.7 million in 2025), Turkey (87.7 million), India (1,463.8 million), Pakistan (255.2 million), Mexico (131.9 million), Iran (92.4 million) and China (1,416.1 million) experience a notable transition from low categories (PSNG based on precipitation information alone; Fig. 3) to high values under both low- and high-emission scenarios (Extended Data Fig. 7 and Supplementary Fig. 16). As a result, Urban region emerges as an additional physiographic region in which more than half of physiographic regions rank as high PSNG (Supplementary Fig. 6), underscoring their pivotal role in shaping monitoring infrastructure requirements, especially the high demand for fine-scale water cycle monitoring in densely populated areas[61].

At the country level, 171 countries are identified as urgently needing new precipitation gauges under SSP5-8.5 (n = 156 for SSP1-2.6; Supplementary Fig. 17). Furthermore, wealthier countries in Asia show strong correlations between GDP and PSNG under SSP5-8.5 (correlation coefficient ≥0.8; Supplementary Fig. 18), indicating Earth observation infrastructure investment could also be maximized in developed countries as a low-risk, high-reward international opportunity. Using the entropy method calculated from different time resolution (either 1900–2022 or 1990–2022) and spatial resolution (0.5°, 2.5°, 5°) yields consistent PSNG results for both SSP1-2.6 and SSP5-8.5 (Extended Data Fig. 7 and Supplementary Figs. 16, 18, 19).

Summary and future work

Our findings highlight important gaps in the global precipitation observation network, including gaps in monsoon affected regions, and low- and mid-latitude areas due to precipitation variability and socioeconomic vulnerabilities, and that reflect regional disparities that undermine climate resilience monitoring. For instance, across tropical Africa, the sparse distribution of stations limits the accuracy of drought and food security early warning systems, especially for severe drought conditions[75] and limits the ability to provide comprehensive drought assessments[76], which could be mitigated with new gauges and enhanced data sharing. Alternatively, at the physiographical scale, gauge density in urban regions falls below WMO standards, which limits the reliability of urban water security and agricultural early warning systems because available gauges are insufficient to capture fine-scale extreme precipitation events amid rapid urbanization and increased flooding[77]. Increasing evidence of a pronounced urban–rural disparity in extreme precipitation[78,79] further elevates societal risk, collectively heightening vulnerability, resulting in high-priority areas in urban regions. Therefore, targeted investment in station deployment is not only a scientific priority but also an urgent social imperative. This study provides insight into where those investments are most urgently needed.

Although this study provides valuable insights, some challenges remain unexplored. First, tailored strategies are essential for regions with poor data sharing or sparse stations. For instance, developed countries with existing infrastructure could establish collaborative data-sharing platforms that are led by national governments, supported by provincial agencies and facilitated by international organizations to integrate diverse datasets into public databases with appropriate licenses, as demonstrated by the DataMart service of Canada and the provincial Pacific Climate Data Set, which archives and disseminates data from a broad range of observing networks in British Columbia. Funding and training in deploying, managing and curating data from low-cost sensor networks provided by international organizations could help developing nations to improve their monitoring and data-sharing abilities. Second, the global station distribution is geographically biased towards lower elevations, with high-altitude regions such as the Qinghai-Tibet Plateau, where orographic effects are critical and very heavily under-represented (representative errors in elevation estimation at the grid level are shown in Supplementary Fig. 20). Addressing this bias would improve hydrometeorological in headwater regions for rivers that provide much of the surface freshwater of the world and would enhance understanding of pivotal systems such as the Asian water tower[80]. Finally, although satellite and reanalysis data provide valuable coverage in data-sparse regions, they cannot substitute for ground-based rain gauges, which are essential for validation. This is exemplified in Africa, where the scarcity of rain gauge data makes it impossible to evaluate the accuracy of satellite-based precipitation products.

Our study also underscores that gaps in the in situ monitoring network fundamentally hinder water cycle and climate change assessment. Therefore, fostering global cooperation to enhance data sharing and establish new stations in the priority regions identified here is imperative to addressing this challenge.

Online content

Any methods, additional references, Nature Portfolio reporting summaries, source data, extended data, supplementary information, acknowledgements, peer review information; details of author contributions and competing interests; and statements of data and code availability are available at https://doi.org/10.1038/s41586-026-10300-5.

1. Stokstad, E. Scarcity of rain, stream gages threatens forecasts. *Science* **285**, 1199–1200 (1999).
2. Kidd, C. et al. So, how much of the Earth's surface is covered by rain gauges? *Bull. Am. Meteorol. Soc.* **98**, 69–78 (2017).
3. Milly, P. C.D., Dunne, K. A. & Vecchia, A. V. Global pattern of trends in streamflow and water availability in a changing climate. *Nature* **438**, 347–350 (2005).
4. McDermid, S. et al. Irrigation in the earth system. *Nat. Rev. Earth Environ.* **4**, 435–453 (2023).
5. Vörösmarty, C. J. et al. Global threats to human water security and river biodiversity. *Nature* **467**, 555–561 (2010).
6. Syed, T. H., Famiglietti, J. S., Chambers, D. P., Willis, J. K. & Hilburn, K. Satellite-based global-ocean mass balance estimates of interannual variability and emerging trends in continental freshwater discharge. *Proc. Natl Acad. Sci. USA* **107**, 17916–17921 (2010).
7. Ham, Y.-G. et al. Anthropogenic fingerprints in daily precipitation revealed by deep learning. *Nature* **622**, 301–307 (2023).
8. Huang, Z., Tan, X., Gan, T. Y., Liu, B. & Chen, X. Thermodynamically enhanced precipitation extremes due to counterbalancing influences of anthropogenic greenhouse gases and aerosols. *Nat. Water* **1**, 614–625 (2023).
9. Tan, X. et al. Increasing global precipitation whiplash due to anthropogenic greenhouse gas emissions. *Nat. Commun.* **14**, 2796 (2023).
10. Pendergrass, A. G., Knutti, R., Lehner, F., Deser, C. & Sanderson, B. M. Precipitation variability increases in a warmer climate. *Sci. Rep.* **7**, 17966 (2017).
11. Li, C. et al. Changes in annual extremes of daily temperature and precipitation in CMIP6 models. *J. Clim.* **34**, 3441–3460 (2021).
12. Thackeray, C. W., Hall, A., Norris, J. & Chen, D. Constraining the increased frequency of global precipitation extremes under warming. *Nat. Clim. Change* **12**, 441–448 (2022).
13. World Meteorological Organization. *State of the Global Climate 2021* (WMO, 2022).
14. Barichivich, J. et al. Recent intensification of Amazon flooding extremes driven by strengthened Walker circulation. *Sci. Adv.* **4**, eaat8785 (2018).
15. Huang, X., Swain, D. L. & Hall, A. D. Future precipitation increase from very high resolution ensemble downscaling of extreme atmospheric river storms in California. *Sci. Adv.* **6**, eaba1323 (2020).
16. Pendergrass, A. G. et al. Flash droughts present a new challenge for subseasonal-to-seasonal prediction. *Nat. Clim. Change* **10**, 191–199 (2020).
17. Yin, J. & Slater, L. J. E. Increase in drought–heatwave events worsens socio-economic productivity and carbon uptake. *Nat. Sustain.* **6**, 241–242 (2023).
18. Yin, J. et al. Future socio-ecosystem productivity threatened by compound drought–heatwave events. *Nat. Sustain.* **6**, 259–272 (2023).

19. Moazami, S., Golian, S., Kavianpour, M. R. & Hong, Y. Uncertainty analysis of bias from satellite rainfall estimates using copula method. *Atmos. Res.* **137**, 145–166 (2014).
20. Yang, Q., Dai, Q., Han, D., Zhu, Z. & Zhang, S. Uncertainty analysis of radar rainfall estimates induced by atmospheric conditions using long short-term memory networks. *J. Hydrol.* **590**, 125482 (2020).
21. Muto, Y. & Kotsuki, S. Estimating global precipitation fields from rain gauge observations using local ensemble data assimilation. *Hydrol. Earth Syst. Sci.* **28**, 5401–5417 (2024).
22. Li, S. et al. Multivariate interpolation and information entropy for optimizing raingauge network in the Mekong River Basin. *Hydrol. Sci. J.* **64**, 1439–1452 (2019).
23. Yang, Z. et al. Bias adjustment of satellite-based precipitation estimation using gauge observations: A case study in Chile. *J. Geophys. Res. Atmos.* **121**, 3790–3806 (2016).
24. Beck, H. E. et al. Daily evaluation of 26 precipitation datasets using Stage-IV gauge-radar data for the CONUS. *Hydrol. Earth Syst. Sci.* **23**, 207–224 (2019).
25. Habib, E., Haile, A. T., Tian, Y. & Joyce, R. J. Evaluation of the high-resolution CMORPH satellite rainfall product using dense rain gauge observations and radar-based estimates. *J. Hydrometeorol.* **13**, 1784–1798 (2012).
26. Ghajarnia, N., Kalantari, Z. & Destouni, G. Data-driven worldwide quantification of large-scale hydroclimatic covariation patterns and comparison with reanalysis and Earth system modeling. *Water Resour. Res.* **57**, e2020WR029377 (2021).
27. Sun, Q. et al. A Review of global precipitation data sets: data sources, estimation, and intercomparisons. *Rev. Geophys.* **56**, 79–107 (2018).
28. Villarini, G., Mandapaka, P. V., Krajewski, W. F. & Moore, R. J. Rainfall and sampling uncertainties: a rain gauge perspective. *J. Geophys. Res. Atmos.* **113**, D11102 (2008).
29. Sadeghi, M. et al. PERSIANN-CNN: precipitation estimation from remotely sensed information using artificial neural networks–convolutional neural networks. *J. Hydrometeorol.* **20**, 2273–2289 (2019).
30. Lanza, L. G. & Stagi, L. Certified accuracy of rainfall data as a standard requirement in scientific investigations. *Adv. Geosci.* **16**, 43–48 (2008).
31. Xie, P. & Arkin, P. A. Analyses of global monthly precipitation using gauge observations, satellite estimates, and numerical model predictions. *J. Clim.* **9**, 840–858 (1996).
32. Huffman, G. J. et al. The new version 3.2 global precipitation climatology project (GPCP) monthly and daily precipitation products. *J. Clim.* **36**, 7635–7655 (2023).
33. Hannah, D. M. et al. Large-scale river flow archives: importance, current status and future needs. *Hydrol. Process.* **25**, 1191–1200 (2011).
34. Zandler, H., Haag, I. & Samimi, C. Evaluation needs and temporal performance differences of gridded precipitation products in peripheral mountain regions. *Sci. Rep.* **9**, 15118 (2019).
35. Riggs, R. M. et al. Extending global river gauge records using satellite observations. *Environ. Res. Lett.* **18**, 064027 (2023).
36. Lenderink, G. & van Meijgaard, E. Unexpected rise in extreme precipitation caused by a shift in rain type? *Nat. Geosci.* **2**, 373 (2009).
37. King, A. D., Reid, K. J. & Saunders, K. R. Communicating the link between climate change and extreme rain events. *Nat. Geosci.* **16**, 552–554 (2023).
38. Zhang, Y. et al. Skilful nowcasting of extreme precipitation with NowcastNet. *Nature* **619**, 526–532 (2023).
39. Zhou, S. et al. Diminishing seasonality of subtropical water availability in a warmer world dominated by soil moisture–atmosphere feedbacks. *Nat. Commun.* **13**, 5756 (2022).
40. Orth, R. & Destouni, G. Drought reduces blue-water fluxes more strongly than green-water fluxes in Europe. *Nat. Commun.* **9**, 3602 (2018).
41. Zhang, Q. et al. Water limitation regulates positive feedback of increased ecosystem respiration. *Nat. Ecol. Evol.* **8**, 1870–1876 (2024).
42. Panagos, P. et al. Global rainfall erosivity assessment based on high-temporal resolution rainfall records. *Sci. Rep.* **7**, 4175 (2017).
43. Li, D. et al. Exceptional increases in fluvial sediment fluxes in a warmer and wetter High Mountain Asia. *Science* **374**, 599–603 (2021).
44. Althoff, D. & Destouni, G. Global patterns in water flux partitioning: irrigated and rainfed agriculture drives asymmetrical flux to vegetation over runoff. *One Earth* **6**, 1246–1257 (2023).
45. Zhou, K. et al. Urban flood risk management needs nature-based solutions: a coupled social-ecological system perspective. *npj Urban Sustain.* **4**, 25 (2024).
46. Renard, D. & Tilman, D. National food production stabilized by crop diversity. *Nature* **571**, 257–260 (2019).
47. Destouni, G., Jaramillo, F. & Prieto, C. Hydroclimatic shifts driven by human water use for food and energy production. *Nat. Clim. Change* **3**, 213–217 (2013).
48. Senande-Rivera, M., Insua-Costa, D. & Miguez-Macho, G. Spatial and temporal expansion of global wildland fire activity in response to climate change. *Nat. Commun.* **13**, 1208 (2022).
49. Zhang, W. et al. Recent decrease of the impact of tropical temperature on the carbon cycle linked to increased precipitation. *Nat. Commun.* **14**, 965 (2023).
50. Gatti, L. V. et al. Increased Amazon carbon emissions mainly from decline in law enforcement. *Nature* **621**, 318–323 (2023).
51. Brandsma, T. *Comparison of Automatic and Manual Precipitation Networks in the Netherlands*. Report No. TR-347 (Royal Netherlands Meteorological Institute, 2014).
52. Overeem, A. *Climatology of Extreme Rainfall from Rain Gauges and Weather Radar*. PhD thesis, Wageningen Univ. (2009).
53. China focus: China forges ahead with meteorological modernization. *China Daily* https://global.chinadaily.com.cn/a/202303/23/WS641c1327a31057c47ebb62fb.html (2023).
54. Rodda, J. C. Guide to hydrological practices. *Hydrol. Sci. J.* **56**, 196–197 (2011).
55. World Meteorology Organization in *International Meteorological Vocabulary* 182–784 (WMO, 1992).
56. Bertini, C. et al. An entropy-based approach for the optimization of rain gauge network using satellite and ground-based data. *Hydrol. Res.* **52**, 620–635 (2021).
57. Bring, A. & Destouni, G. Arctic climate and water change: model and observation relevance for assessment and adaptation. *Surv. Geophys.* **35**, 853–877 (2014).
58. Vousdoukas, M. I. et al. Small island developing states under threat by rising seas even in a 1.5 °C warming world. *Nat. Sustain.* **6**, 1552–1564 (2023).
59. Pathirana, A. Small islands: living laboratories revealing global climate and sustainable development challenges. *Front. Clim.* **6**, 2024 (2025).
60. Mildenberger, M. et al. How publics in small-island states view climate change and international responses to it. *Proc. Natl Acad. Sci. USA* **122**, e2415324122 (2025).
61. Hemmati, M., Kornhuber, K. & Kruczkiewicz, A. Enhanced urban adaptation efforts needed to counter rising extreme rainfall risks. *npj Urban Sustain.* **2**, 16 (2022).
62. Rodríguez-Fonseca, B. et al. Variability and predictability of West African droughts: a review on the role of sea surface temperature anomalies. *J. Clim.* **28**, 4034–4060 (2015).
63. Mohtadi, M., Prange, M. & Steinke, S. Palaeoclimatic insights into forcing and response of monsoon rainfall. *Nature* **533**, 191–199 (2016).
64. Mulitza, S. et al. Synchronous and proportional deglacial changes in Atlantic meridional overturning and northeast Brazilian precipitation. *Paleoceanogr. Paleoclimatol.* **32**, 622–633 (2017).
65. Bintanja, R. & Andry, O. Towards a rain-dominated Arctic. *Nat. Clim. Change* **7**, 263–267 (2017).
66. McCrystall, M. R., Stroeve, J., Serreze, M., Forbes, B. C. & Screen, J. A. New climate models reveal faster and larger increases in arctic precipitation than previously projected. *Nat. Commun.* **12**, 6765 (2021).
67. Liu, Q., Bader, J., Jungclaus, J. H. & Matei, D. More extreme summertime North Atlantic oscillation under climate change. *Commun. Earth Environ.* **6**, 474 (2025).
68. Serreze, M. C., Barrett, A. P. & Lo, F. Northern high-latitude precipitation as depicted by atmospheric reanalyses and satellite retrievals. *Mon. Weather Rev.* **133**, 3407–3430 (2005).
69. Rawlins, M. A. & Karmalkar, A. V. Regime shifts in arctic terrestrial hydrology manifested from impacts of climate warming. *Cryosphere* **18**, 1033–1052 (2024).
70. Bring, A. et al. Arctic terrestrial hydrology: a synthesis of processes, regional effects, and research challenges. *J. Geophys. Res. Biogeosci.* **121**, 621–649 (2016).
71. van der Schrier, G., Overeem, A. & Verver, G. *Improving Access to Sub-Daily Rain Gauge Data Citation* https://insitu.copernicus.eu/resources/library/improving-access-to-sub-daily-rain-gauge-data-may-2021 (Copernicus, 2021).
72. Lin, J. et al. Making China's water data accessible, usable and shareable. *Nat. Water* **1**, 328–335 (2023).
73. Gu, L. et al. Large anomalies in future extreme precipitation sensitivity driven by atmospheric dynamics. *Nat. Commun.* **14**, 3197 (2023).
74. Le, P. V. V. et al. Climate-driven changes in the predictability of seasonal precipitation. *Nat. Commun.* **14**, 3822 (2023).
75. Masih, I., Maskey, S., Mussá, F. E. F. & Trambauer, P. A review of droughts on the African continent: a geospatial and long-term perspective. *Hydrol. Earth Syst. Sci.* **18**, 3635–3649 (2014).
76. Huang, S. et al. Widespread global exacerbation of extreme drought induced by urbanization. *Nat. Cities* **1**, 597–609 (2024).
77. Rentschler, J. et al. Global evidence of rapid urban growth in flood zones since 1985. *Nature* **622**, 87–92 (2023).
78. Liu, S. et al. More heavy precipitation in world urban regions captured through a two-way subgrid land-atmosphere coupling framework in the NCAR CESM2. *Geophys. Res. Lett.* **51**, e2024GL108747 (2024).
79. Su, J., Miao, C., Hu, J., Wu, Y. & Ji, J. Widening urban–rural precipitation differences in China: regionally varied intensification since 2000. *Earths Future* **13**, e2025EF006657 (2025).
80. Zhang, Q. et al. Oceanic climate changes threaten the sustainability of Asia's water tower. *Nature* **615**, 87–93 (2023).

Methods

This study integrates daily gauge observations, CMIP6 model outputs and socioeconomic data to evaluate global precipitation monitoring gaps and identify global priority regions for new gauge deployment. The methodology consists of four main components: (1) compiling and harmonizing a multi-source precipitation gauge dataset to map current global observational coverage; (2) constructing a physiography-based reference map and quantifying network deficiencies; (3) linking historical gauge placement priorities to existing gauge density and precipitation spatial variability; and (4) projecting future priority areas under various climate and socioeconomic scenarios using a target-based simulation framework. To ensure the robustness of model outputs and main conclusions, we evaluate the results through sensitivity analysis using multiple spatial windows and validate the priority sites for new gauges.

Input data

Precipitation gauge network. We compiled a global precipitation gauge network comprising 245,368 stations from 15 daily gauge-based precipitation datasets (Supplementary Table 1; for details, see Supplementary Text 1). Among these, 14,505 gauges were relocated several times. To ensure data accuracy and eliminate duplication, we consolidated and deduplicated stations based on location (0.001°), resulting in a final dataset of 221,483 unique stations. A subset of 38,203 LR stations was identified for a duration exceeding 30 years and having less than 10% missing data over the entire observed record[1]. Although precipitation data were collected from 1850 onwards, our analysis mainly focused on the spatial and temporal distributions of all stations and LR stations during the period 1900–2022 because of high data gaps in the nineteenth century. Station densities were calculated on a 1° × 1° grid following the WMO standards (Supplementary Table 3).

CMIP6 model data. We obtained monthly climate variables from 13 Coupled Model Intercomparison Project Phase 6 (CMIP6) models (Supplementary Table 4) because they provided output with the necessary variables for the historical period (1850–2014) and future projections (2015–2100) under various scenarios. Five key variables include: precipitation flux (pr), near-surface (2 m) air temperature (tas), water evapotranspiration flux (evspsbl), relative humidity (hur) and total emission rate of black carbon aerosol mass (emibc). We used historical simulations for the period 1970–1999 and future projections for 2025–2100 under two scenarios: a low-emission pathway (SSP1-2.6) and a high-emission (SSP5-8.5) pathway. All variables were uniformly reprocessed to a standardized 1° × 1° grid using bilinear interpolation.

Future economic and population data. We used global gridded population data (person per km^2) with a 30-arc-second resolution from ref. 81, covering 2025–2100 under the Sustainability pathway (SSP1) and Fossil fuelled development (SSP5) scenarios. Global GDP data (in 2005 US dollars, purchasing power parity) from ref. 82 were similarly gridded and time-matched. Both datasets were aggregated into a 1° × 1° grid by average.

Mapping physiographical regions

The global physiographic map (Supplementary Fig. 3) includes seven regions: Interior Plains (labelled as Plains in figures), Hilly/Undulating, Mountains, Coastal Zones (Coastal), Small Islands (Islands), Urban Areas (Urban) and Polar/Arid regions. We used the 2015 Global Ecological Land Units database[83] (GELU) with a 250-m resolution for most regions, supplemented by the Global, Self-consistent, Hierarchical, High-resolution Shoreline database[84] (GSHHS) and the Global Islands Database[85] (GID). We then aggregated the original resolution of the physiographic map to 1° × 1° by maintaining the dominant class within each grid cell. With special consideration given to the Urban region, where the grids containing more than 2.5% urban region were classified as belonging to the Urban region (details in Supplementary Text 2 and Supplementary Fig. 21). This resulted in 15,390 grid cells, excluding Antarctica, which formed the basis for our analyses.

Information for prioritizing new gauge siting

We identified priority areas for siting new precipitation gauges based on three sets of information: (1) historical precipitation characteristics; (2) projected future precipitation trends; and (3) anticipated socioeconomic development. A detailed conceptual framework is presented in Extended Data Fig. 3.

Historical precipitation characteristics. The historical precipitation characteristic was implemented by introducing two factors: gauge density (GD) and precipitation spatial variability. GD was calculated using all available stations (n = 221,483) from 1900 to 2022. It represents a local deficiency of gauge, regions with already high GD require fewer additional gauges. Precipitation spatial variability was evaluated using daily data from LR stations (n = 38,203) over the same period, high spatial variability in precipitation calls for denser gauge coverage, such as in monsoon regions, which experienced high precipitation variations. Daily records from non-LR stations were excluded due to substantial gaps.

To quantify the spatial variability, we introduced the maximum information minimum redundancy (MIMR) criterion, which quantifies the need for new gauges by favouring stations that provide high information and low redundancy relative to their neighbours[86–88]. The MIMR decomposes into two components: marginal entropy (H; Supplementary Text 3, Eq. (2)), which measures the information from each gauge, and mutual information (T; Supplementary Text 3, Eq. (3)), which quantifies redundancy from nearby stations[86] (see Venn diagrams in Supplementary Fig. 22 and details in Supplementary Text 3). Mutual information were calculated using dynamic windows of various sizes of 0.5°, 1°, 2.5° and 5°. We then calculated the MIMR using the formula:

$$\mathrm{MIMR} = \mathrm{norm}(H) + (-\mathrm{norm}(T)) \quad (1)$$

where norm denotes the min–max normalization process, which standardizes H and T to eliminate differences in entropy arising from varying discretization or resolution[89]. MIMR takes values in the range of −1 to 1, with a higher value indicating greater informational value with lower redundancy.

Projected future precipitation trends. To extend precipitation variability into a future context, we incorporated uncertainties in CMIP6-based precipitation trend projections under SSP1-2.6 and SSP5-8.5. The goal was to identify areas in which climate space is most under-represented (areas characterized by precipitation projections are both important and highly uncertain), thereby warranting enhanced ground-based monitoring. Future precipitation under-representation builds on the established link between missing observations and uncertain future trends: incomplete local precipitation observations lead to incomplete climate model representation, high inter-model variability and persistent projection uncertainty[90]. This uncertainty can be reduced by closing observational gaps in measurement networks.

To quantify the future precipitation trends, we adjusted the absolute error (AE)[90] metric, which quantify the trend disagreement between CMIP6-projected precipitation and machine-learning predictions. Specifically, we treated the CMIP6-projected precipitation during 2025–2100 (under a given SSP) as a pseudo-observation. We then trained a Random Forest (RF) model[91], using the same set of CMIP6 predictors, to independently estimate precipitation in each grid cell (detailed below). The AE was calculated as the absolute difference between the RF-predicted and CMIP6 trends. Higher AE values reflect greater model–predictor mismatch and therefore lead to poorly constrained or validated model projections of models, signal a higher

priority for improved observational support. This metric transform projection uncertainty into spatial guidance of gauges, addressing a limitation of conventional CMIP6 inter-comparisons that show parametric differences (for example, standard deviation) but fail to diagnose climatically underrepresented zones.

Central to this approach is training the RF model only in grid cells with existing in situ gauges, ensuring that the machine-learning model learns relationships between climate predictors and precipitation in regions in which historical gauge-based observations exist. This design enables reliable climate–space extrapolation while highlighting regions in which climate features (for example, precipitation variability) are inadequately sampled. Once trained, the RF model was applied globally to estimate future precipitation trends in all grid cells. These model-free estimates were then compared against the CMIP6 model projections, yield multi-model median AE from 13 CMIP6 models under both SSP1-2.6 and SSP5-8.5 (detailed in Supplementary Text 4, see simplified diagrams in Supplementary Fig. 23). To construct the RF model, we began by selecting four key predictors based on existing literature[92–97]: near-surface air temperature (tas), evapotranspiration (evspsbl), relative humidity (hur), and the total emission rate of black carbon aerosol mass (emibc). These variables are widely recognized as important drivers of long-term changes in precipitation. To reduce multicollinearity and improve model interpretability, we conducted a predictor screening step. Among the four variables, air temperature and evapotranspiration emerged as the most informative. These two predictors alone explained more than 80% of the spatial variation in CMIP6 precipitation across the globe (Supplementary Text 5 and Supplementary Figs. 24–26).

Socioeconomic development. We estimated future socioeconomic conditions by including projected population density and GDP from 2025 to 2100 under SSP1 (for SSP1-2.6) and SSP5 (for SSP5-8.5). Socioeconomic development represents the areas where citizens have high need and where countries can support the constructing new stations or maintaining existing equipment.

Multicriteria incorporation algorithm

To identify the priority areas for siting new gauges (denoted as PSNG) score, we applied two objective weighting methods: principal component analysis (PCA)[98], which assigns weights based on the variance explained by each principal component, and the entropy weight method (EWM)[99], which evaluates how controlling factors affect the result and measures the uncertainty of variables (Supplementary Texts 6–7). Both methods determine weights from the data structure without relying on subjective assumptions that can be solved over a range of relative weights to understand how these components trade-off. We used averaged weights driven by PCA and EWM methods as the robust final weight of factors (GD and MIMR, AE, population density and GDP) due to this synthesis, dispersion-based information content (from EWM) with variance-structure considerations (from PCA), and the weights obtained from PCA and EWM were similar (see Supplementary Fig. 27, further details of PSNG and weights comparisons are provided in the Supplementary Text 8). The function is

$$\text{Priority}_i = \sum_{1}^{j} W_j \times \text{Var}_{j,i} \quad (2)$$

where Priority_i is the PSNG score for grid cell i, and W_j is the weight of factors j (Var_j).

For historical PSNG, we incorporated GD and MIMR ($\text{Priority}_{\text{his},i}$, Supplementary Text 8, Eq. (20)), we also recalculated the PSNG using data from 1990 to 2022 to assess the sensitivity of the results to recent climate trends. For future PSNG when consider precipitation projections and socioeconomic development under future scenarios, we incorporated GD and MIMR, AE, population density and GDP into the final future prioritization framework ($\text{Priority}_{\text{fut},i}$, Supplementary Text 8, Eq. (21)). To isolate the effects from precipitation on PSNG, we additionally evaluated the combined influence of historical and future precipitation variability by integrating the GD, MIMR and AE metrics ($\text{Priority}_{\text{pr},i}$, Supplementary Text 8, Eq. (22)). All five components were normalized by their maximum values before aggregation and weighted using a combined PCA and EWM approach. To better understanding factors leading to high PSNG, we decompose the PSNG into the contributions from its factors in each country (Supplementary Text 8, Eq. (23)).

Visualizing priority ranking

To visualize global PSNG considering different conditions, we used a percentile ranking method to establish an eight-level scale. The percentile thresholds used for assigning ranks were 1%, 15%, 30%, 45%, 60%, 75% and 90% of the original values. The priority levels for siting new gauges in the future precipitation and socioeconomic changes under SSP1-2.6 and SSP5-8.5 scenario ($\text{Priority}_{\text{fut},i}$, $\text{Priority}_{\text{pr},i}$) were determined based on the same percentile thresholds as those derived from the historical precipitation condition ($\text{Priority}_{\text{his},i}$). This allows a direct comparison of priority rankings across different scenarios and helps identify areas with changing needs for precipitation gauge infrastructure in response to various precipitation and socioeconomic changes. Our primary analyses were conducted at a 1° × 1° spatial resolution, with additional tests performed at 0.5°, 2.5° and 5° resolutions. These results, shown in the Supplementary Information, provide robust validation of our findings.

Validation of priority sites for new gauges

To validate the PSNG using historical precipitation data—given the absence of independent future gauge observations—we propose that reducing the number of gauges decreases the mutual information shared among stations, thereby increasing the PSNG values. We tested this assumption in North America, which offers a high density of LR stations suitable for systematic resampling. We evaluated the stability and robustness of PSNG by progressively subsampling the network, retaining 80%, 60%, 40%, 20%, 10%, 5% and 1% of the original LR stations. For each subsampled network, we recalculated PSNG and assessed its spatial consistency (Extended Data Fig. 5, Supplementary Text 9 and Supplementary Fig. 8).

Reporting summary

Further information on research design is available in the Nature Portfolio Reporting Summary linked to this article.

Data availability

The precipitation gauge data sources are summarized in Supplementary Table 1. The CMIP6 data are available at https://www.wcrp-climate.org/wgcm-cmip/wgcmcmip6. The GELU data are available at https://rmgsc.cr.usgs.gov/outgoing/ecosystems/global/. The GSHHS data can be found at https://www.ngdc.noaa.gov/mgg/shorelines/data/gshhg/latest/. The GID data can be found at https://rmgsc.cr.usgs.gov/outgoing/ecosystems/global/. The source data are available at Zenodo (https://doi.org/10.5281/zenodo.18364510) (ref. 100). Source data are provided with this paper.

Code availability

The codes to reproduce the study are available at Zenodo (https://doi.org/10.5281/zenodo.18364510) (ref. 100).

81. Wang, X., Meng, X. & Long, Y. Projecting 1 km-grid population distributions from 2020 to 2100 globally under shared socioeconomic pathways. *Sci. Data* **9**, 563 (2022).
82. Wang, T. & Sun, F. Global gridded GDP data set consistent with the shared socioeconomic pathways. *Sci. Data* **9**, 221 (2022).
83. Sayre, R. et al. *A New Map of Global Ecological Land Units—An Ecophysiographic Stratification Approach* 46 (Association of American Geographers, 2014).

84. Wessel, P. & Smith, W. H. F. A global, self-consistent, hierarchical, high-resolution shoreline database. *J. Geophys. Res. Solid Earth* **101**, 8741–8743 (1996).
85. Sayre, R. et al. A new 30 meter resolution global shoreline vector and associated global islands database for the development of standardized ecological coastal units. *J. Oper. Oceanogr.* **12**, S47–S56 (2019).
86. Shannon, C. E. A mathematical theory of communication. *Bell Syst. Tech. J.* **27**, 379–423 (1948).
87. Fahle, M., Hohenbrink, T. L., Dietrich, O. & Lischeid, G. Temporal variability of the optimal monitoring setup assessed using information theory. *Water Resour. Res.* **51**, 7723–7743 (2015).
88. Li, C., Singh, V. P. & Mishra, A. K. Entropy theory-based criterion for hydrometric network evaluation and design: maximum information minimum redundancy. *Water Resour. Res.* **48**, W05521 (2012).
89. Ruddell, B. L. & Kumar, P. Ecohydrologic process networks: 1. Identification. *Water Resour. Res.* **45**, W03419 (2009).
90. Bessenbacher, V., Gudmundsson, L. & Seneviratne, S. I. Optimizing soil moisture station networks for future climates. *Geophys. Res. Lett.* **50**, e2022GL101667 (2023).
91. Breiman, L. Random forests. *Mach. Learn.* **45**, 5–32 (2001).
92. Pendergrass, A. G. & Hartmann, D. L. Global-mean precipitation and black carbon in AR4 simulations. *Geophys. Res. Lett.* **39**, L01703 (2012).
93. Thorpe, L. & Andrews, T. The physical drivers of historical and 21st century global precipitation changes. *Environ. Res. Lett.* **9**, 064024 (2014).
94. Richardson, T. B. et al. Drivers of precipitation change: an energetic understanding. *J. Clim.* **31**, 9641–9657 (2018).
95. Sand, M., Samset, B. H., Tsigaridis, K., Bauer, S. E. & Myhre, G. Black carbon and precipitation: an energetics perspective. *J. Geophys. Res. Atmos.* **125**, e2019JD032239 (2020).
96. Clemens, S. C. et al. Remote and local drivers of Pleistocene South Asian summer monsoon precipitation: a test for future predictions. *Sci. Adv.* **7**, eabg3848 (2021).
97. Myhre, G. et al. Scientific data from precipitation driver response model intercomparison project. *Sci. Data.* **9**, 123 (2022).
98. Hastie, T., Tibshirani, R., & Friedman, J. *The Elements of Statistical Learning: Data Mining, Inference, and Prediction* 2nd edn (Springer, 2009).
99. Wu, R. M. X. & Wang, Y. Which objective weight method is better: PCA or entropy? *Sci. J. Res. Rev.* **3**, SJRR.MS.ID.000558 (2022).
100. Su, J. J. Precipitation observing network gaps limit climate change impact assessment (R script). *Zenodo* https://doi.org/10.5281/zenodo.18364510 (2026).

Acknowledgements C.M. acknowledges support from the National Natural Science Foundation of China (42521001, U24A20572), the National Key Research and Development Program of China (2024YFF0809301), and the 111 Project of China (B23027). L.V.A. is funded by Australian Research Council (ARC) grants FT210100459 and CE230100012. G.D. acknowledges support from the Swedish Research Council (VR, project grant 2022-04672). We acknowledge the dataset contributor for kindly providing the gauge data in support of the analysis. Continent and country boundary layers were sourced from Esri ArcGIS Living Atlas (ArcGIS Online).

Author contributions J.S., C.M. and F.Z. conceived and designed the study. J.S. led the model development and conducted the simulations. J.S., C.M. performed the analyses with support from H.B., P.J., Q.S., L.S., W.R.B., Y. Wada, D.R., J.G., Y. Wu, P.T., P.B., P.P., L.V.A., Q.Z., J.H., S.-K.M., L.J.S., Q.D., G.D., J.A.M., R.M., S.S., H.B., P.J., Q.S. and L.S. interpreted the results, J.S., C.M. and F.Z. wrote the paper with input from all co-authors.

Competing interests The authors declare no competing interests.

Additional information

Supplementary information The online version contains supplementary material available at https://doi.org/10.1038/s41586-026-10300-5.

Correspondence and requests for materials should be addressed to Chiyuan Miao.

Peer review information *Nature* thanks the anonymous reviewers for their contribution to the peer review of this work. Peer reviewer reports are available.

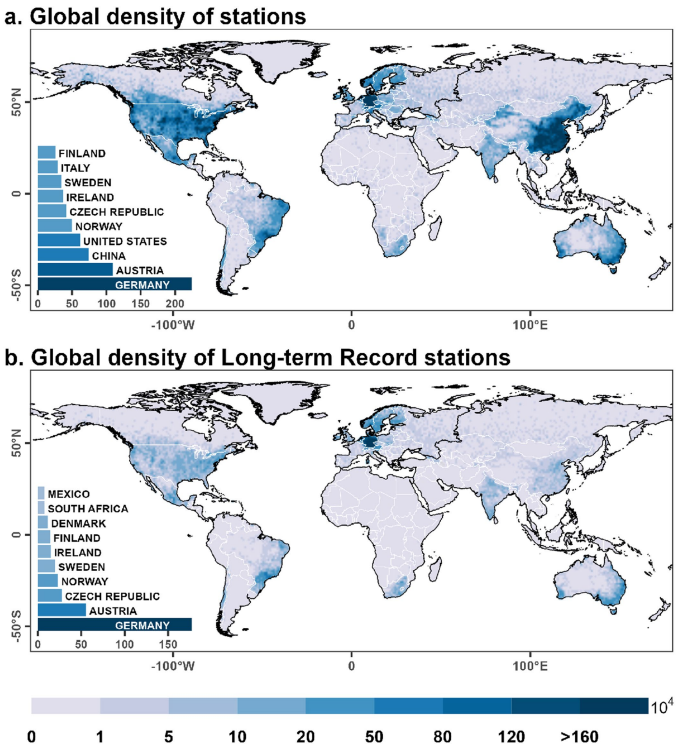

Extended Data Fig. 1 | Collected daily precipitation gauge density from 1900 to 2022. (a) Station density (total N = 221,483 gauges, see Methods). (b) Long-term Record station density (N = 38,203 gauges). The unit is station numbers per area (stations per km^2). The inset plots show the top 10 countries by station density, with areas larger than 50,000 km^2. Gauge density is based on a 1° × 1° grid for the period 1900–2022. Map image is the intellectual property of Esri and is used herein under license. Copyright © 2026 Esri and its licensors. All rights reserved.

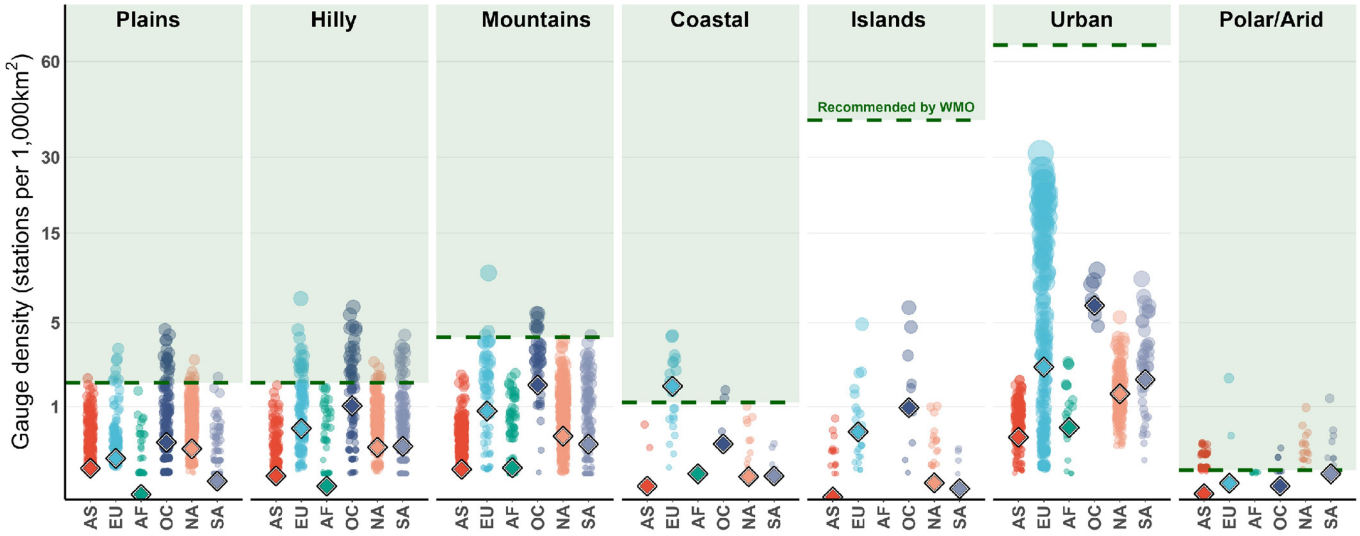

Extended Data Fig. 2 | Global Long-term Record precipitation gauge density during 1900–2022 compared with WMO standards. Bubbles indicate the grid-cell gauge densities, while diamonds represent the mean density for each continent and physiographic region. Horizontal dashed green lines represent WMO's minimum density recommendations for each physiographic region. Continental abbreviations are follows: AS = Asia, EU = Europe, AF = Africa, OC = Oceania, NA = North America, SA = South America. Gauges density is based on a 1° × 1° grid for the period 1900–2022.

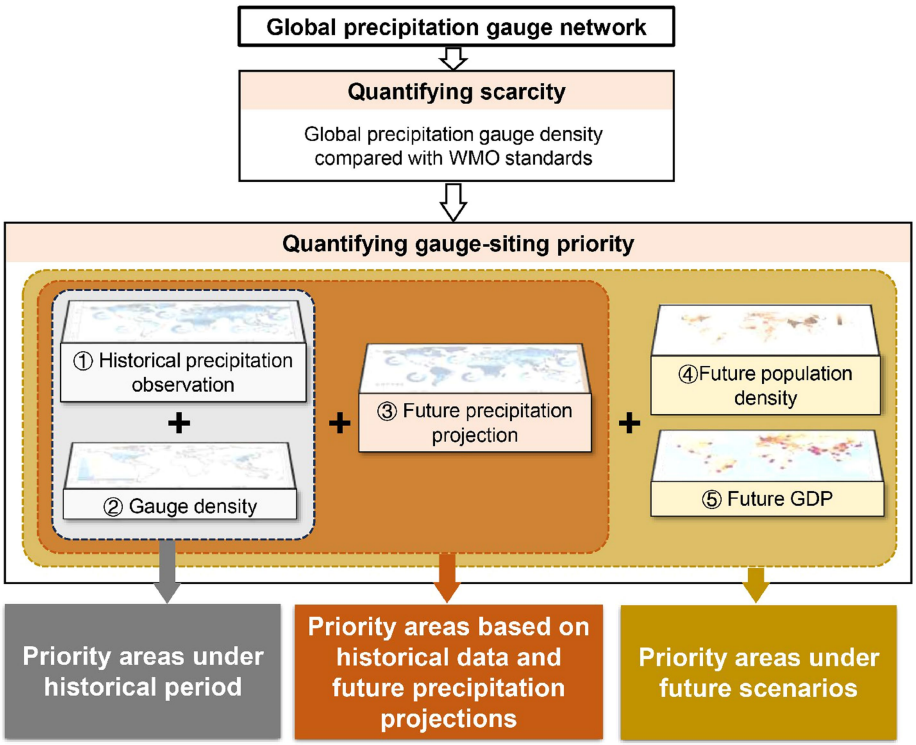

Extended Data Fig. 3 | Framework for analyzing global priority level for siting new gauges. The framework comprises three key components: collecting gauge data, quantifying scarcity and quantifying gauge-siting priority.

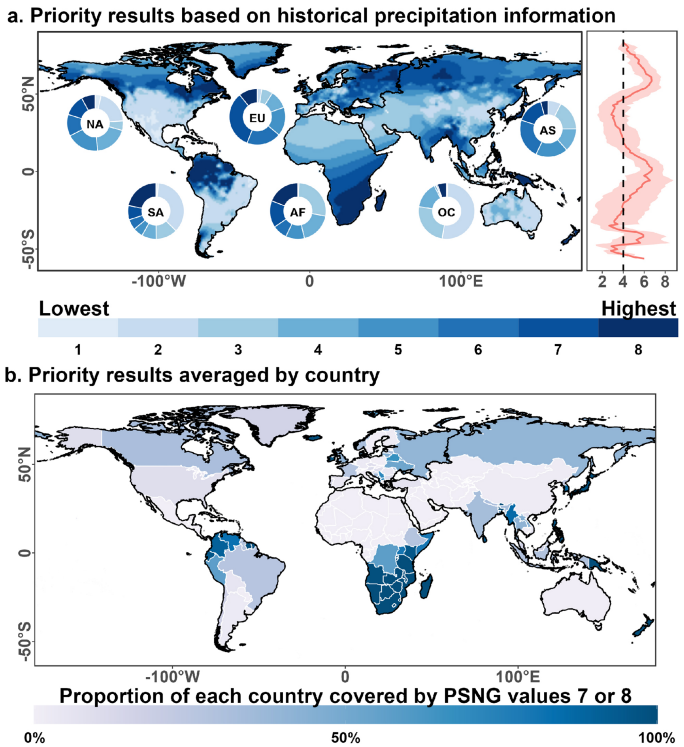

Extended Data Fig. 4 | Global priority for siting new gauges under historical period (1990–2022). (a) The inset pie charts show the relative proportion of each PSNG level across continents. The red line in right represents the mean PSNG by latitude, with shading for mean ± one standard deviation. Continental abbreviations are follows: AS = Asia, EU = Europe, AF = Africa, OC = Oceania, NA = North America, SA = South America. (b) Proportion of each country covered by PSNG levels 7–8. Map image is the intellectual property of Esri and is used herein under license. Copyright © 2026 Esri and its licensors. All rights reserved.

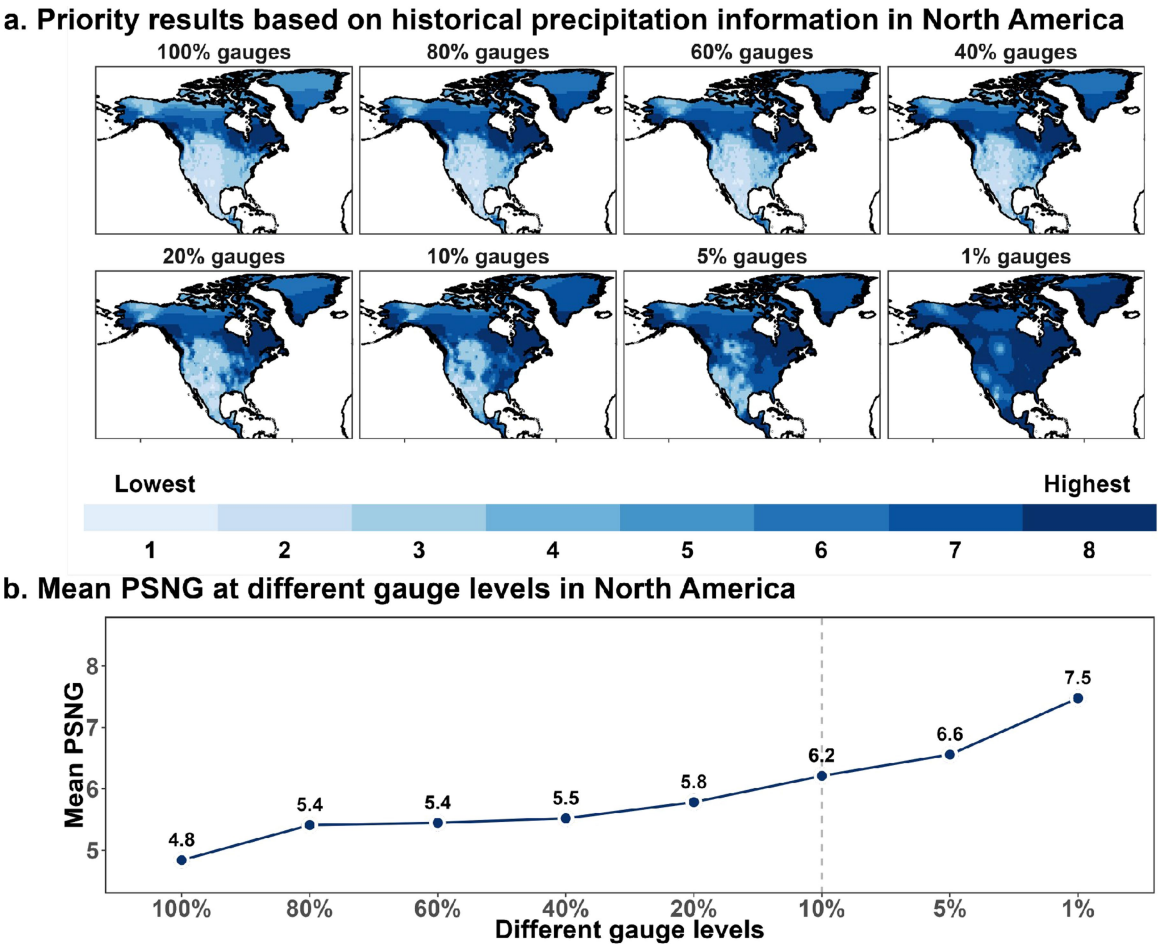

Extended Data Fig. 5 | Priority for siting new gauges under historical period (1900–2022) at different retained gauge levels in North America. (a) The spatial distribution of priority areas in North America. (b) Mean priority results at different retained gauge levels in North America. Map image is the intellectual property of Esri and is used herein under license. Copyright © 2026 Esri and its licensors. All rights reserved.

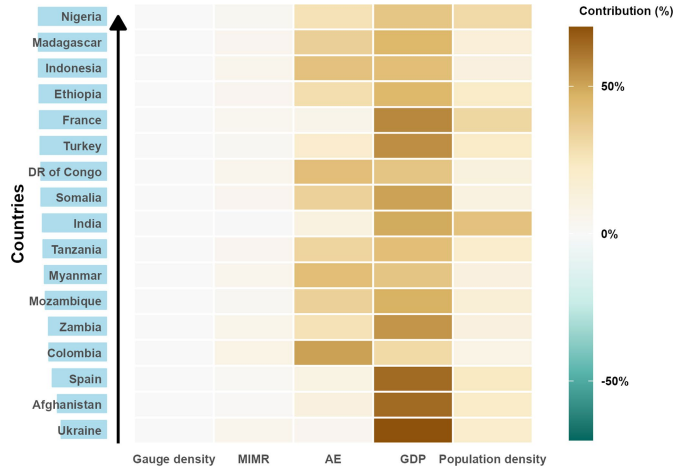

Extended Data Fig. 6 | Factors contributing to future PSNG under SSP5-8.5 scenario. The bar plot showing the top 15 largest countries (over 500,000 km^2) ranked by the proportion of their area classified as high priority (PSNG scores 7–8, the blue length indicates the proportion).

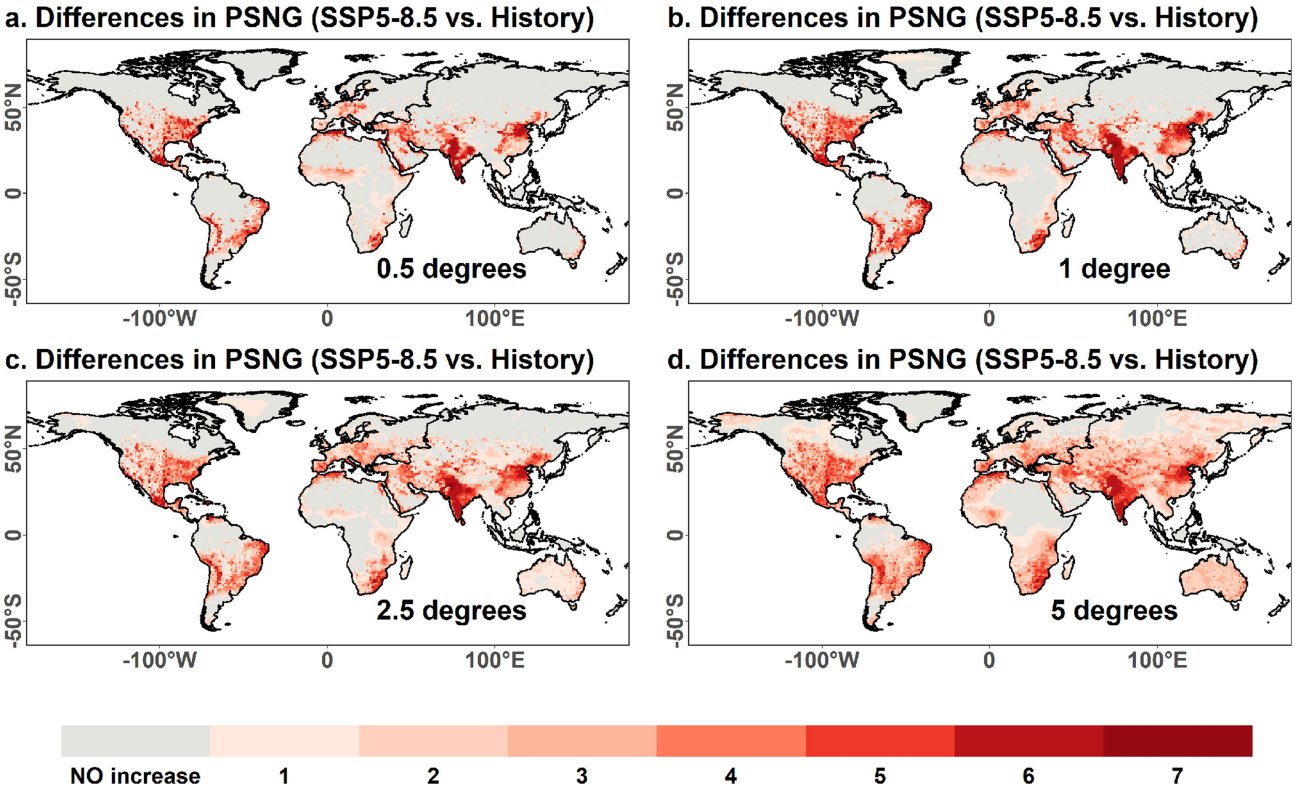

Extended Data Fig. 7 | Differences in PSNG between future SSP5-8.5 and historical periods when aggregating data at (a) 0.5°, (b) 1°, (c) 2.5°, and (d) 5° resolution.

nature portfolio

Corresponding author(s): DAPR, 2025-07-18553C

Last updated by author(s): Feb 17, 2026

Reporting Summary

Nature Portfolio wishes to improve the reproducibility of the work that we publish. This form provides structure for consistency and transparency in reporting. For further information on Nature Portfolio policies, see our Editorial Policies and the Editorial Policy Checklist.

Statistics

For all statistical analyses, confirm that the following items are present in the figure legend, table legend, main text, or Methods section.

n/a	Confirmed
☒	☐ The exact sample size (*n*) for each experimental group/condition, given as a discrete number and unit of measurement
☒	☐ A statement on whether measurements were taken from distinct samples or whether the same sample was measured repeatedly
☒	☐ The statistical test(s) used AND whether they are one- or two-sided *Only common tests should be described solely by name; describe more complex techniques in the Methods section.*
☒	☐ A description of all covariates tested
☐	☒ A description of any assumptions or corrections, such as tests of normality and adjustment for multiple comparisons
☐	☒ A full description of the statistical parameters including central tendency (e.g. means) or other basic estimates (e.g. regression coefficient) AND variation (e.g. standard deviation) or associated estimates of uncertainty (e.g. confidence intervals)
☐	☒ For null hypothesis testing, the test statistic (e.g. *F*, *t*, *r*) with confidence intervals, effect sizes, degrees of freedom and *P* value noted *Give P values as exact values whenever suitable.*
☒	☐ For Bayesian analysis, information on the choice of priors and Markov chain Monte Carlo settings
☒	☐ For hierarchical and complex designs, identification of the appropriate level for tests and full reporting of outcomes
☐	☒ Estimates of effect sizes (e.g. Cohen's *d*, Pearson's *r*), indicating how they were calculated

Our web collection on statistics for biologists contains articles on many of the points above.

Software and code

Policy information about availability of computer code

Data collection	Source data are provided via Zenodo: https://doi.org/10.5281/zenodo.18364510.
Data analysis	Codes to reproduce the study are available via Zenodo at https://doi.org/10.5281/zenodo.18364510

For manuscripts utilizing custom algorithms or software that are central to the research but not yet described in published literature, software must be made available to editors and reviewers. We strongly encourage code deposition in a community repository (e.g. GitHub). See the Nature Portfolio guidelines for submitting code & software for further information.

Data

Policy information about availability of data

All manuscripts must include a data availability statement. This statement should provide the following information, where applicable:

- Accession codes, unique identifiers, or web links for publicly available datasets
- A description of any restrictions on data availability
- For clinical datasets or third party data, please ensure that the statement adheres to our policy

The precipitation gauge data sources are summarized in Supplementary Table 1. The CMIP6 data are available at https://www.wcrp-climate.org/wgcm-cmip/wgcmcmip6. The GELU data are available at https://rmgsc.cr.usgs.gov/outgoing/ecosystems/global/. The GSHHS data can be found at https://www.ngdc.noaa.gov/mgg/shorelines/data/gshhg/latest/. The GID data can be found at https://rmgsc.cr.usgs.gov/outgoing/ecosystems/global/. Source data are provided via Zenodo: https://doi.org/10.5281/zenodo.18364510.

Research involving human participants, their data, or biological material

Policy information about studies with human participants or human data. See also policy information about sex, gender (identity/presentation), and sexual orientation and race, ethnicity and racism.

Reporting on sex and gender	*Use the terms sex (biological attribute) and gender (shaped by social and cultural circumstances) carefully in order to avoid confusing both terms. Indicate if findings apply to only one sex or gender; describe whether sex and gender were considered in study design; whether sex and/or gender was determined based on self-reporting or assigned and methods used.* *Provide in the source data disaggregated sex and gender data, where this information has been collected, and if consent has been obtained for sharing of individual-level data; provide overall numbers in this Reporting Summary. Please state if this information has not been collected.* *Report sex- and gender-based analyses where performed, justify reasons for lack of sex- and gender-based analysis.*
Reporting on race, ethnicity, or other socially relevant groupings	*Please specify the socially constructed or socially relevant categorization variable(s) used in your manuscript and explain why they were used. Please note that such variables should not be used as proxies for other socially constructed/relevant variables (for example, race or ethnicity should not be used as a proxy for socioeconomic status).* *Provide clear definitions of the relevant terms used, how they were provided (by the participants/respondents, the researchers, or third parties), and the method(s) used to classify people into the different categories (e.g. self-report, census or administrative data, social media data, etc.)* *Please provide details about how you controlled for confounding variables in your analyses.*
Population characteristics	*Describe the covariate-relevant population characteristics of the human research participants (e.g. age, genotypic information, past and current diagnosis and treatment categories). If you filled out the behavioural & social sciences study design questions and have nothing to add here, write "See above."*
Recruitment	*Describe how participants were recruited. Outline any potential self-selection bias or other biases that may be present and how these are likely to impact results.*
Ethics oversight	*Identify the organization(s) that approved the study protocol.*

Note that full information on the approval of the study protocol must also be provided in the manuscript.

Field-specific reporting

Please select the one below that is the best fit for your research. If you are not sure, read the appropriate sections before making your selection.

☐ Life sciences ☐ Behavioural & social sciences ☒ Ecological, evolutionary & environmental sciences

For a reference copy of the document with all sections, see nature.com/documents/nr-reporting-summary-flat.pdf

Ecological, evolutionary & environmental sciences study design

All studies must disclose on these points even when the disclosure is negative.

Study description	This study involved computational analysis and modelling of publicly available datasets.
Research sample	No research samples were used in this study.
Sampling strategy	No sampling was undertaken in this study.
Data collection	This study collected fifteen daily gauge-based precipitation datasets, all data sources were available and are described in detail in the Supplementary Information, Table 1, along with URLs to the original source repositories.
Timing and spatial scale	The gauge data was collected during period 1900–2022.
Data exclusions	No data were excluded from analysis.
Reproducibility	All work comprised computational analysis and is fully reproducible given the code base and input datasets.
Randomization	This study did not require any randomization procedure.
Blinding	This study did not require any blinding procedures.

Did the study involve field work? ☐ Yes ☒ No

Reporting for specific materials, systems and methods

We require information from authors about some types of materials, experimental systems and methods used in many studies. Here, indicate whether each material, system or method listed is relevant to your study. If you are not sure if a list item applies to your research, read the appropriate section before selecting a response.

Materials & experimental systems

n/a	Involved in the study
☒	☐ Antibodies
☒	☐ Eukaryotic cell lines
☒	☐ Palaeontology and archaeology
☒	☐ Animals and other organisms
☒	☐ Clinical data
☒	☐ Dual use research of concern
☒	☐ Plants

Methods

n/a	Involved in the study
☒	☐ ChIP-seq
☒	☐ Flow cytometry
☒	☐ MRI-based neuroimaging

Plants

Seed stocks	No plants or seed stocks were required for this study.
Novel plant genotypes	No plants or seed stocks were required for this study.
Authentication	No plants or seed stocks were required for this study.